

THE UNIVERSITY OF WARWICK

Original citation:

Tian, Y., Liu, C., Liu, Xianping, Wang, F., Li, X., Qin, Y., Zhang, D. and Shirinzadeh, B. (2015) Design, modelling and characterization of a 2-DOF precision positioning platform. Transactions of the Institute of Measurement and Control, 37 (3). pp. 396-405.

Permanent WRAP url:

<http://wrap.warwick.ac.uk/74984>

Copyright and reuse:

The Warwick Research Archive Portal (WRAP) makes this work by researchers of the University of Warwick available open access under the following conditions. Copyright © and all moral rights to the version of the paper presented here belong to the individual author(s) and/or other copyright owners. To the extent reasonable and practicable the material made available in WRAP has been checked for eligibility before being made available.

Copies of full items can be used for personal research or study, educational, or not-for-profit purposes without prior permission or charge. Provided that the authors, title and full bibliographic details are credited, a hyperlink and/or URL is given for the original metadata page and the content is not changed in any way.

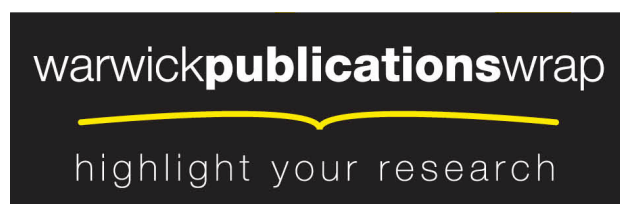
Publisher's statement:

<http://dx.doi.org/10.1177/0142331214540692>

A note on versions:

The version presented here may differ from the published version or, version of record, if you wish to cite this item you are advised to consult the publisher's version. Please see the 'permanent WRAP url' above for details on accessing the published version and note that access may require a subscription.

For more information, please contact the WRAP Team at: wrap@warwick.ac.uk



<http://go.warwick.ac.uk/lib-publications>

Design, modeling and characterization of a 2-DOF precision positioning platform

Y. Tian¹, C. Liu¹, X. Liu², F. Wang¹, X. Li¹, Y. Qin¹, D. Zhang¹, B. Shirinzadeh³

¹Key Laboratory of Mechanism Theory and Equipment Design of Ministry of Education, Tianjin University, Tianjin 300072, China

²School of Engineering, University of Warwick, Coventry CV4 7AL, UK

³Robotics and Mechatronics Research Laboratory, Department of Mechanical and Aerospace Engineering, Monash University, Clayton 3800, Australia

Abstract: This paper presents the mechanical design, parameter optimization and experimental tests of a 2-DOF (Degree of Freedom) flexure-based precision positioning platform, which has great potential application in many scientific and engineering fields. During the mechanical design, the leaf parallelogram structures provide the functions of joint mechanisms and transmission mechanisms with excellent decoupling property. The dynamic model of the developed positioning platform is established and analyzed using PRBM (Pseudo Rigid Body Model) methodology. A PSO (Particle Swarm Algorithm) optimization approach is utilized to perform the parameter optimization and thus improve the static and dynamic characteristics of the positioning platform. The prototype of the developed 2-DOF positioning platform has been fabricated using WEDM (Wire Electric Discharge Machining) technique. A number of experimental testing has been conducted to investigate the performance of the platform and verify the established models and optimization methodologies. The experimental results show that the platform has a workspace range in excess of $8.0\mu\text{m}\times 8.0\mu\text{m}$ with the stiffness of $4.97\text{ N}/\mu\text{m}$ and the first order natural frequency of 231 Hz. The cross-axis coupling ratio is less than 0.6%, verifying the excellent decoupling performance.

Keywords: precision positioning platform; PRBM; PSO optimization approach; flexure hinge; laser based measurement

1. Introduction

Micro/nano precision positioning platform is widely used in the industrial and academic areas to conduct leading-edge scientific research (Verma et al., 2005; Tian et al., 2009a). The prospective and versatile applications include precision manipulations (Qin et al., 2013a), atomic force microscope (Greco et al., 2013), scanning tunneling microscope (Tian et al., 2009b), optical fiber alignment (Lee et al., 2011), single molecule experiment in physics (Zheng et al., 2013) and micro-assembly (Tian et al., 2011a). Recent advances in scientific and engineering applications show increasing demands in positioning accuracy, resolution, response speed, workspace and stability of such kinds of instruments and devices (Casciati et al., 2013; Ang et al., 2013). The flexure-based micro/nano positioning platform has obtained a considerable amount of attentions for the advantages including free of backlash, wear and friction (Hopkins et al., 2012; Tian et al., 2010; Tian et al., 2009c; Tian et al., 2011b; Bhagat et al., 2013), and thus it has been considered as one of the best candidates for conducting the high accuracy positioning from several nanometer to hundreds of micrometers.

There are two kinds of configurations for the 2-DOF (Degree of Freedom) positioning platform, namely, serial mechanism (Friedman et al., 2010) and parallel mechanism (Li et al., 2012a; Xu, 2014). The design of the serial platform is straightforward, however, its positioning error will be accumulated, thus affecting the motion accuracy of the platform. In addition, the serial configuration will also increase the mass of the moving part, and thus reduce the response speed of the platform. On the contrary, the parallel platform shows distinct advantages in terms of rigidity, accuracy, load capacity and identical performance in each axis. Hence, parallel mechanisms are more preferable and attract more attentions in the past few years. However, the output cross-axis decoupling is one of the challenges in the design of parallel mechanism, which increases the complexity of the design and modeling of the mechanism. The output cross-axis decoupling means one actuator only drives the central

stage in one axial direction without affecting the other direction. For PEA (Piezoelectric Actuator) is weak to the lateral force and bending, thus large coupling will damage the PEA. However, the coupling ratio of traditional mechanisms is between 1% and 1.5% mechanism (Li et al., 2012b; Xu, 2014). Thus it is important to develop the design methodology for mechanisms with negligible cross-axis couplings.

Parallelogram-based mechanisms can be used to overcome the cross-axis couplings, which include leaf hinge parallelogram and circular hinge parallelogram (Li et al., 2011; Qin et al., 2013b). For a parallelogram-based flexure mechanism, it works as a transmission mechanism in the longitudinal direction due to the large axial stiffness, and a joint in transverse direction due to the small out-of-plane stiffness (Li et al., 2012b). Compared with the circular hinge mechanism, the leaf hinge mechanism can implement large working range, low stress concentration, and small dimension. Thus it is more suitable for the compact platform design with large bandwidth.

The mechanical structure of the positioning platform plays a main role in the static and dynamic performance of the micro/nano positioning platform. Thus, a suitable optimization approach should be used to make the first natural frequency of the platform meet the requirements of the high bandwidth. A number of approaches including PSO (Particle Swarm Algorithm), GA (Genetic Algorithm) have been proposed to optimize the parameters of the micro/nano positioning platform (Lin et al., 2012). It is demonstrated that the PSO approach is robust and efficient to conduct the parameter optimization, since it has no evolutionary operators including crossover and mutation. Thus it is generally utilized to optimize the structure of the platform.

The mechanical design, parameters optimization methodologies of a 2-DOF precision positioning platform featuring the parallelogram decoupling mechanisms have been developed. The dynamic model of the developed positioning platform has been established

based on PRBM technique. PSO optimization approach is utilized to optimize the geometric parameters and thus improve the static and dynamic characteristics of the developed platform. The platform can provide a workspace range in excess of $8.0\ \mu\text{m}\times 8.0\ \mu\text{m}$ with a natural frequency of 231 Hz, the across axis coupling ratio is less than 0.6%, indicating the excellent decoupling performance. The main contributions of this paper are as follows: 1) The mechanical design and optimization methodologies for such kinds of compact planar positioning platforms have been established. 2) The cross-axis decoupling has been significantly improved, compared with previous designs.

2. Mechanical design

The schematic diagram of the 2-DOF precision positioning platform is shown in Fig.1. This platform is symmetric design, and thus reducing the effects of the thermal deformation and external disturbance on the platform. In the proposed platform, the central moving part is connected to the dual Parallel Leaf-Spring Mechanisms (PLSM) through a set of leaf parallelogram mechanisms. These leaf parallelogram mechanisms include two types of configurations: type *A* is joint mechanism and type *B* transmission mechanism. The stiffness of the leaf parallelogram is large in the longitudinal direction and low in the transverse direction. Therefore, as shown in Fig.1, when the PEA in the *Y* axis is activated, the leaf parallelograms in the *Y* axis (type *B*) translate the motion to the central moving part due to the large stiffness in the *Y* axis. The leaf parallelogram in the *X* axis (type *A*) works as a joint due to its low rigidity in the *Y* axis. In addition, the PEA in the *Y* axis only drives the central platform in *Y* direction without affecting the *X* direction and thus the PEA is free from bending and lateral forces. The platform is designed with a half cylinder between the PEA and the dual PLSM to form Hertzian contact and thus further reduce/eliminate the bending force acting on the PEA. The working principle of the platform in the *X* direction is similar with that in the *Y* direction due to the symmetric design in the *X* and *Y* directions. Aluminum alloy

T7075 is chosen to construct the platform due to its high strength properties. The Young's Modulus is 70 Gpa, Poisson ratio is 0.33 and the density is 2700 kg/m³. The WEDM (Wire Electric Discharge Machining) technique is utilized to fabricate the flexure-based mechanism to guarantee the machining accuracy and the performance of the developed positioning platform.

3. PRBM modeling

As shown in Fig. 2, the dual PLSM combines the advantages of the conventional parallelogram and double four-bar parallelogram. It has the capability of providing larger displacement, smaller stress concentration and motion decoupling. As demonstrated in Fig.2(a), L and b represent the length and width of the translational link, respectively, l and t are the length and width of the PRBM link, respectively. Fig.2(b) shows the equivalent static model of the dual PLSM. In addition, as show in Fig.2(c), the leaf parallelogram can provide pure translation motion in the Y direction without affecting transverse directional motion in the X direction. The thickness of the dual PLSM is denoted by d .

PRBM technique is a common solution in the design of flexure-based mechanism. In traditional kinematics theory, it is assumed that all links are completely rigid and/or relatively small deformable. PRBM technique replaces flexure-based link with rigid link and torsional springs and remains the load-displacement relationships similar between the flexure-based mechanism and the PRBM model. Thus, the computational accuracy and efficiency can be guaranteed for the modeling of flexure-based mechanism.

3.1 Modeling of the leaf hinge

Fig.3 shows the principle of the PRBM technique. Deformation of the cantilevered leaf hinge under external load is shown in Fig. 3(a). It is noted that the leaf hinge will deflect when the free end is subjected to the vertical force. The curve of the leaf hinge can be determined by the continuous mechanics. Fig.3(b) shows the PRBM model of the leaf hinge.

There are two rigid bodies connected with a spring, which denotes the rotational stiffness of the flexure-based link. In the PRBM model, the deflection of the free end is equal to that of the leaf hinge determined by continuous mechanics. The length of the rotational link is γl , where γ is the parameter to determine the deflection characteristics and trajectory of the free end of the leaf hinge.

As shown in Fig. 3(b), the deflection of the PRBM link is induced by tangential force F_t , and thus the torque acting at the spring can be expressed as follows:

$$T = k\theta \quad (1)$$

where k is the rotational stiffness of flexure-based link, θ is the rotational angle of PRBM link.

The torque can also be expressed as follows:

$$T = F_t \gamma l \quad (2)$$

where F_t is tangential force, γ is PRBM coefficient, and l is the length of the leaf flexure hinge.

From mechanics point of view, it can be obtained:

$$k_\theta \theta = \frac{F_t l^2}{EI} \quad (3)$$

where k_θ is the coefficient of rotational stiffness, E is the modulus of elasticity, I is the moment of inertia.

Substituting Eqs. (1) and (2) into Eq. (3), the rotational stiffness of the flexure-based link can be expressed as:

$$k = k_\theta \gamma \frac{EI}{l} \quad (4)$$

3.2 Modeling of the platform

The 2-DOF precision positioning platform has symmetry structures in the X and Y directions, and thus the dynamic models of the X and Y axes are same. For simplicity and

without loss generality, the dynamic model in the X direction is developed based on the PRBM technique and Lagrange's equation methodology. Accordingly, the first order natural frequency is obtained and analyzed.

Based on the Newton's motion law, the kinetic energies of positioning platform are given as follows:

1) The kinetic energy of connected link

$$T_1 = 4 \times \frac{1}{2} m_3 (\gamma l)^2 \dot{\theta}_1^2 \quad (5)$$

2) The kinetic energy of PRBM link

$$T_2 = 8 \times \left[\frac{1}{2} m_2 \left(\frac{\gamma l \dot{\theta}_1}{2} \right)^2 + \frac{1}{2} J \dot{\theta}_1^2 \right] \\ + 8 \times \left[\frac{1}{2} m_2 \left(\frac{1}{2} \gamma l \dot{\theta}_1 + \gamma l \dot{\theta}_1 \right)^2 + \frac{1}{2} J \dot{\theta}_1^2 \right] \quad (6)$$

3) The kinetic energy of translational link

$$T_3 = 2 \times \frac{1}{2} m_1 \times [2\gamma l \dot{\theta}_1]^2 \quad (7)$$

4) The kinetic energy of type B hinge

$$T_4 = 4 \times \frac{1}{2} m_2 (2\gamma l \dot{\theta}_1)^2 \quad (8)$$

5) The kinetic energy of type A hinge

$$T_5 = 4 \times \left[\frac{1}{2} m_2 \left(\frac{2\gamma l \dot{\theta}_1}{2} \right)^2 + \frac{1}{2} J (2\dot{\theta}_1)^2 \right] \quad (9)$$

6) The kinetic energy of moving part

$$T_6 = \frac{1}{2} m_4 (2\gamma l \dot{\theta}_1)^2 \quad (10)$$

Thus, the total kinetic energy of the platform can be obtained as:

$$T_0 = T_1 + T_2 + T_3 + T_4 + T_5 + T_6 \\ = (4m_1 + 20m_2 + 2m_3 + 2m_4) \cdot (\gamma l)^2 \cdot \dot{\theta}_1^2 + 16J \dot{\theta}_1^2 \quad (11)$$

where m_i ($i=1, 2, 3, 4$) denotes the mass of translational link, PRBM link, connected link and

central platform, respectively, J is the moment of inertia of PRBM link, θ_1 is the angular displacement about the Z axis, as shown in Fig.4.

The potential energy of the platform is obtained as follows:

$$\begin{aligned} U &= \sum_{i=1}^{32} \frac{1}{2} k \theta_1^2 + \sum_{i=1}^8 \frac{1}{2} k (2\theta_1)^2 = 32k\theta_1^2 \\ &= 32\gamma k_\theta \frac{EI}{l} \theta_1^2 \end{aligned} \quad (12)$$

The Lagrange's equation is given as follows:

$$\frac{d}{dt} \left(\frac{\partial T}{\partial \dot{\theta}_1} \right) - \frac{\partial T}{\partial \theta_1} + \frac{\partial U}{\partial \theta_1} = -c\dot{\theta}_1 \quad (13)$$

where c is the damping coefficient.

Substituting Eqs. (11) and (12) into Eq. (13), the governing equation of motion of the platform can be given as follows:

$$\begin{aligned} & \left[(8m_1 + 40m_2 + 4m_3 + 4m_4) \cdot (\gamma l)^2 + 32J \right] \ddot{\theta}_1 \\ & + c\dot{\theta}_1 + 64\gamma k_\theta \frac{EI}{l} \theta_1 = 0 \end{aligned} \quad (14)$$

Then, the stiffness of platform in the Y direction can be expressed as follows:

$$K = \frac{64k_\theta EI}{\gamma l^3} \quad (15)$$

The first order natural frequency in the Y direction can be given as follows:

$$f = \frac{4}{\pi} \sqrt{\frac{\gamma k_\theta EI}{\left[(8m_1 + 40m_2 + 4m_3 + 4m_4) \cdot (\gamma l)^2 + 32J \right] l}} \quad (16)$$

4. PSO optimization

The PSO optimization approach is utilized to perform the optimization. The flowchart of PSO method is shown in Fig. 5. PSO is an optimization approach based on iterative method, compared with GA, its advantages include no crossover and no mutation, and thus there are fewer parameters to be regulated and it is easy to perform. The optimization process is given as follows:

- 1) The computational system initializes velocity and position of all particles.
- 2) The system evaluates all particles, putting every particle's optimal velocity and optimal position into P_{best} .
- 3) Comparing all particles' optimal velocity and position, the system will put best velocity and best position into g_{best} .
- 4) Updating all velocity and position in g_{best} via PSO formula.
- 5) Comparing all particles' velocity and position which have been updated with all particles' optimal velocity and position which are stored in g_{best} . If the system is not satisfied with any particle, go back to step 2 and regenerate new particles until one satisfied particle is found. This particle is the optimal design.

In the Step 4, the PSO formula can be expressed as follows:

$$\begin{aligned}
 v_{i,j}(t+1) &= wv_{i,j}(t) + c_1r_1[p_{i,j} - x_{i,j}(t)] + c_2r_2[p_{i,j} - x_{i,j}(t)] \\
 x_{i,j}(t+1) &= x_{i,j}(t) + v_{i,j}(t+1)
 \end{aligned} \tag{17}$$

In the PSO formula, the parameters c_1 and c_2 are the learning factors, w denotes the weight function, r_1 and r_2 are random numbers distributes uniformly in the range from 0 to 1. The accuracy of the PSO approach is highly dependent on the parameters of the PSO formula including number of particles, learning factors, weight function, motion range and dimensions of particles. The number of particles is highly dependent on the complexity of the problem, for general optimization problem, 20-40 particles are suitable, if number of the particles is excessive, it will extend the optimization time and decrease the optimization efficiency. On the contrary, the optimization accuracy can not be guaranteed. The weight function w makes a well balance between the capability of expanding in all search space and exploring in local space. The learning factor c_1 is related to expanding capability, while c_2 is related to exploring capability. If the value of c_1 is too large, particle moves only in local space, but not in all search space, if the value of c_2 is too large, the optimization result will converge to minimum,

which degrades the optimization accuracy.

As shown in Fig.2(a), the design variables for the platform are: L , b , l and t . The objective function is the first natural frequency in the Y direction devoted as f . The geometric and physic parameters of the platform are shown in Table 1. Based on the given parameters and the PSO optimization approach, the mechanical design optimization of the positioning platform can be performed. The convergent process of the PSO optimization is shown in Fig. 6. The optimal value search stops at the 50 generation. Fig. 6(a) shows the convergent process of the best and average fitness values. It is noted that the best fitness value can reach up to the final value at generation 6 and keep constant during the further generation. The mean fitness will also drops to the final value at generation 10, but slightly fluctuates near the final value when the generation increases. The average distance between the individuals is shown in Fig. 6(b). It can be seen that the value of the average distance generally decreases with the increasing of the generation. After generation 25, the average distance reaches up to the minimal value and remains constant till the stop of the optimization, which indicates the convergent stability of the PSO optimization. Fig.6(c) shows the particles' distribution. It is noted that most of the particles gathered in the 231.4 Hz, indication that the optimized first order natural frequency of the positioning platform is 231.4 Hz. The corresponding optimized parameters are shown in Table 2. For the purpose of comparison, the optimization results of GA are also provided. It is noted that the obtained values of geometric parameters are slightly deferent between the two optimization methods. However, the PSO optimization method can obtain the higher first natural frequency and thus improve the working bandwidth of the developed precision positioning platform. This is mainly due to the inherent property of PSO optimization, which has no crossover and mutation operators.

Fig.7 shows the relationship between the parameters and the first natural frequency, every parameter is assigned with their initial values and changes in the range of 40%, as

shown in Tab.3. The first natural frequency is normalized to 100 Hz. it can be seen that the parameters t and l have more significant influence on the first order natural frequency than the parameters b and L . The first order natural frequency increases with the increasing t , but decreases with the increasing l , b and L .

Fig.8 shows the influence of the parameters t and l on the first order natural frequency and normalized stiffness. It is noted that the influence of parameter l on the first order natural frequency is more significant than that of parameter t . However, the influence of the parameter l on stiffness is less than that of parameter t . The first order natural frequency and stiffness have similar decreasing trends against increasing parameters t and l , respectively.

It can be seen from Figs.7 and 8 that the first order natural frequency and stiffness are more sensitive to the parameters t and l . In order to develop a high performance positioning platform, it is crucial and important to conduct the parameter optimization of the flexure-based mechanism.

5. Finite element analyses

In order to obtain further insights into the performance of the micro/nano positioning platform, the finite element analysis (FEA) is conducted based on the commercial software ANSYS. According to the optimized geometric parameters, the finite element model is established in ANSYS software, as shown in Fig. 9. The element type is chosen as SOLID 92, which is a 3D 10 node element and each node has 3 translational DOF in the x , y and z directions. In order to improve the computational accuracy, the mapped mesh technique is conducted in the sections of the leaf hinges. Other sections of the platform are meshed using smart and free methodology.

Based on the established finite element model, the static analysis is firstly conducted to obtain the stiffness of the platform in the X and Y directions. Since the stiffness is one of the important parameters to affect the performance of positioning platform. It has influences on

not only the working range of the piezo-driven flexure-based mechanism but also the natural frequency of the entire system. During the static analysis, the constant force with the magnitude of 10 N is applied on the moving part in the X and Y directions, respectively. The corresponding displacement of the moving part is collected during the post process of the FEA. Based on the Hook's law, the static stiffness of the positioning platform can be obtained. From the static finite element analyses, it is noted that the stiffness of the platform is estimated as 4.9 N/ μm . After the static analyses, the modal analysis is performed to extract to first four order mode shapes and the corresponding natural frequencies within the range from 0 Hz to 2 KHz. The first four order mode shapes are shown in Fig.10. Due to the symmetric structure, the first two order mode shapes are the translational motion of the moving part in the Y and X directions with the corresponding natural frequency of 235 Hz. This is also the desired mobility of the positioning platform. The third order mode shape is the rotation of the moving part about the Z axis with natural frequency of 713 Hz. The fourth order mode shape is the translation motion of the moving part in the Z direction with the natural frequency of 1568 Hz. Based on the values of the natural frequencies, it can be concluded that the flexure-based mechanism has a lower stiffness in the desired motion direction, and higher stiffness in other directions. This indicates that the developed positioning platform can implement 2-DOF positioning and have large capability of resisting external disturbance. It must be pointed out that the stiffness in the X and Y directions can be improved by the installed PEAs, and thus the natural frequencies of the positioning platform can be further improved.

6. Experimental tests

In order to examine the performance of the developed positioning platform and verify the established mechanical design and optimization methodologies, a number of experimental tests for static and dynamic characteristics have been conducted.

6.1 Stiffness measurement

Fig.11 shows the experimental setup for the stiffness test. The platform is fixed on the optical table Newport RS-4000. The applied force is measured by a pull push force gauge from ALGOL, and the displacement of the moving part is recorded by laser based sensor from KEYENCE LK-G5000. The applied force increases from 0 N to 20 N with the step of 2 N, and the corresponding displacement of the moving part is measured. In order to eliminate the random error, the measurement procedure is repeated three times. Fig. 12 shows the stiffness testing results. It is noted that the relationship between the applied force and displacement of the moving part of the platform is linear. The stiffness can be calculated based on Hook's law as 4.97 N/ μm . The stiffness comparisons among the analytic computation, FEA and experimental testing are shown in Table 4. It can be seen that there are marginally discrepancy between the obtained results. The error between the analytical method and the experimental test is 1.01% and that between FEA and experimental testing is 1.27%. The errors are mainly due to the theoretical assumptions of flexure hinges and the machining errors of WEDM for the prototype manufacture, as well as the sensing and measurement uncertainty of the experimental measurement system.

6.2 Modal analysis

Fig.13 shows the experimental setup for the modal analysis of the positioning platform. The impact modal analysis is conducted to obtain the natural frequency of the positioning platform. Two B&K accelerometers are mounted on the moving part of the platform to measure the response caused by impact force. An impact hammer provides pulse impact excitation to the platform and a force sensor attached to the hammer is utilized to measure the impact force. The force and corresponding acceleration signals are amplified by a charge amplifier and then sent to the dynamic analyzer instrument. Using the modal analysis software, the FRF (Frequency Response Function) of the developed positioning platform can

be obtained. In order to reduce the random errors, the average method is adopted to improve the testing accuracy. A low-pass filter with cutoff frequency of 1 KHz is utilized to eliminate the external disturbance. Fig.14 shows the obtained experimental results. Due to the geometric symmetry, the dynamic characteristics in the X and Y directions are almost the same. The first curve peak corresponds to the first and second order mode shapes with frequency of 231 Hz, and the second curve peak denotes the third mode shape with frequency of 720 Hz. The first two mode shapes are the translations of the moving platform in the X and Y direction respectively. The third mode shape is the rotation of the moving platform about the Z axis. For simplification and without loss generality, Table5 shows the comparisons of the first order natural frequencies in the X direction among analytic computation, FEA and experimental testing. It is noted that the experimental result is in good agreement with the analytical computation and FEA. The errors between the analytical computation, FEA and experimental tests are respectively 0.87% and 1.73%, respectively. The slight differences mainly result from the manufacturing errors, sensing and measurement uncertainties, and the theoretical assumptions of analytical model. However, the experimental testing can validate the feasibility and reliability of the proposed design and optimization methodologies.

6.3 Workspace test

Fig.15 shows experimental setup for the workspace test. The platform is fixed on the optical table. The PEA is activated by PEA amplifier THORLABS MDT T693A, and the displacement of the moving part is measured by laser based sensor from KEYENCE LK-G5000. The matlab simulink toolbox is used to construct the signal generation and record code, and then the code is downloaded into the dSPACE DS1103 controller, which is used to supply the command signal to the PEA amplifier. The displacement of the moving part is measured by the laser sensor in real time and the measured signal is collected by the dSPACE and fed to the computer for recording. The measured workspace of the developed positioning

platform is shown in Fig. 16, where the maximum voltage applied at the PEA is 100 V, which is less than the nominal maximum driving voltage (150 V) to protect the PEAs. Since the workspace of the developed positioning platform is a square shape, a 2D rectangular trajectory is utilized to examine the reachable workspace of the platform. It is noted that the workspace is in excess of $8.0\ \mu\text{m}\times 8.0\ \mu\text{m}$. The workspace dimension can be further increased by increasing the driving voltage to the maximum values, and the PEAs with larger nominal displacement can further improve the workspace. However, due to the hysteresis of the PEAs, the workspace of the platform is not a regular square. This irregularity may also be induced by the coupling between the two axes.

In order to examine the coupling effect, the PEA in the Y direction is activated, and both the displacement of the moving part in the X and Y directions is recorded and plotted in Fig. 17. The displacement of the moving part in the X direction is considered as the coupling motion. It can be seen from Fig. 17(a) that the hysteresis exists in the trajectory of the moving part under open loop control condition. The maximum difference between the expansion and retraction trajectories is approximately $1.42\ \mu\text{m}$. This hysteresis phenomenon can be reduced/eliminated by closed-loop control methodology and thus improving the positioning accuracy of the developed positioning platform. The maximum coupling motion of the moving part in the X direction is $0.04\ \mu\text{m}$, indicating that the coupling ratio is approximately 0.5%. The coupling ratio in Y direction is about 0.6% when the X direction is activated. These show the excellent decoupling performance of the developed positioning platform.

7. Conclusions

The mechanical optimization design, dynamic modeling and characterization methodologies of a flexure-based mechanism have been conducted. A 2-DOF precision positioning platform is developed based on dual PLSM and the decoupling performance between two translational directions has been realized by use of leaf parallelogram

mechanisms. In order to improve the static and dynamic characteristics of the positioning platform, PSO optimization approach is utilized to improve the dynamic performance. From the FEA results, it is noted that the parameters of the dual PLSM link have significant influences on the first natural frequency and the stiffness of the entire platform. Experimental results show that the platform has a workspace in excess of $8.0\ \mu\text{m}\times 8.0\ \mu\text{m}$ with a stiffness of $4.97\ \text{N}/\mu\text{m}$ and a first natural frequency of 231 Hz, and the coupling ratio is negligible small.

Compared with other 2-DOF mechanisms, the advantage of developed positioning platform is the high position accuracy and low cross-axis coupling ratio (less than 0.6%) due to the dual PLSM structure and geometric symmetric design, which can provide high lateral stiffness for the guide system. The experimental measurement and characterization demonstrate the effectiveness of the proposed mechanical optimization design and modeling methodologies. The obtained key enabling techniques can provide the guidelines for the development of such kinds of compact positioning platform with high decoupling motion capability.

Acknowledgement

This research is supported by National Natural Science Foundation of China (Nos. 51175372, 51275337), National Key Special Project of Science and Technology of China (No. 2011ZX04016-011), Reserved Academic Program of Peiyang Scholar, and Program for New Century Excellent Talents in University (No. NCET-11-0374).

References

- Ang KK, Dai J (2013) Response analysis of high-speed rail system accounting for abrupt change of foundation stiffness. *Journal of Sound and Vibration* 332(12): 2954-2970.
- Bhagat U, Shirinzadeh B, Tian Y, Zhang D (2013) Experimental analysis of laser interferometry-based robust motion tracking control of a flexure-based mechanism. *IEEE Transactions on Automation Science and Engineering* 10(2): 267-275.
- Casciati F, Wu L (2013) Local positioning accuracy of laser sensors for structural health monitoring. *Structural Control & Health Monitoring* 20(5): 728-739.
- Friedman DCW, Kowalewski T, Jovanovic R, Rosen J, Hannaford B (2010) Freeing the serial

- mechanism designer from inverse kinematic solvability constraints. *Applied Bionics and Biomechanics* 7(3): 209-216.
- Greco G, Lanerc TS, Torrassa S (2013) Microtopography of the eye surface of the crab *Carcinus maenas*: an atomic force microscope study suggesting a possible antifouling potential. *Journal of the Royal Society, Interface/the Royal Society* 10(84): 20130122.
- Hopkins JB, Panas RM (2012) Design of flexure-based precision transmission mechanism using screw theory. *Precision Engineering* 37(2): 299-307.
- Lee HS, Park JY, Cha SM (2011) Ribbon plastic optical fiber linked optical transmitter and receiver modules featuring a high alignment tolerance. *Optics Express* 19(5): 4301-4309.
- Li YM, Huang JM, Tang H (2012b) A compliant parallel XY micromotion stage with complete kinematic decoupling. *IEEE Transactions on Automation Science and Engineering* 9(3): 538-553.
- Li YM, Xu QS (2012a) Design and robust repetitive control of a new parallel-kinematic XY piezostage for micro/nano-manipulation. *IEEE/ASME Transactions on Mechatronics* 17(6): 1120-1132.
- Li YM, Xu QS (2011) A novel piezo-actuated XY stage with parallel, decoupled and stacked flexure structure for micro/nano positioning. *IEEE Transactions on Industrial Electronics* 58(8): 3601-3615.
- Lin CJ, Lin PT (2012) Particle swarm optimization based feedforward controller for a XY PZT positioning stage. *Mechatronics* 22(5): 614-628.
- Qin Y, Shirinzadeh B, Zhang D (2013b) Compliance modeling and analysis of statically indeterminate symmetric flexure structures. *Precision Engineering* 37(2): 415-424.
- Qin Y, Tian Y, Zhang D, Shirinzadeh B, Fatikow S (2013a) A novel direct inverse modeling approach for hysteresis compensation of piezoelectric actuator in feedforward applications. *IEEE/ASME Transactions of Mechatronics* 18(3): 981-989.
- Tian Y, Liu X, Zhang D, Chetwynd DG (2009a) Dynamic modeling of the fidelity of random surface measurement by the stylus method. *Wear* 266(5-6): 555-559.
- Tian Y, Shirinzadeh B, Zhang D (2009b) A flexure-based mechanism and control methodology for ultra-precision turning operation. *Precision Engineering* 33(2): 160-166.
- Tian Y, Shirinzadeh B, Zhang D (2009c) A flexure-based five-bar mechanism for micro/nano manipulation. *Sensors and Actuators A: Physical* 153(1): 96-104.
- Tian Y, Shirinzadeh B, Zhang D (2010) Design and dynamics of a 3-DOF flexure-based parallel mechanism for micro/nano Manipulation. *Microelectronic Engineering* 87(2): 230-241.
- Tian Y, Shirinzadeh B, Zhang D, Zhong Y (2011b) Modeling and analysis of a 3RRR parallel micro-positioning mechanism. *PIMEchE Part C, Journal of Mechanical Engineering Science* 255(5): 1027-1043.
- Tian Y, Zhang D, Shirinzadeh B (2011a) Dynamic modeling of a flexure-based mechanism for ultra-precision grinding operation. *Precision Engineering* 35(4): 554-565.

- Verma S, Kin W, Shakir H (2005) Multi-axis maglev nanopositioner for precision manufacturing and manipulation applications. *IEEE Transactions on Industrial Application* 41(5): 1159-1167.
- Xu QS (2014) Design and development of a compact flexure-based XY precision positioning system with centimeter range. *IEEE Transactions on Industrial Electronics* 61(2): 8931-903.
- Zheng Y, Li P, Zhao N (2013) Kinetics of molecular transitions with dynamic disorder in single-molecule pulling experiments. *The Journal of Chemical Physics* 138(20): 204102.

List of figure and table captions

Fig.1 Schematic diagram of the 2-DOF precision positioning platform

Fig.2 PLSM mechanic model

Fig.3 PRBM model of link

Fig.4 Rotational angle θ_1 due to the force F

Fig.5 Flowchart of the PSO optimization approach

Fig.6 PSO optimization process

Fig.7 Relationship between the parameters and the first natural frequency

Fig.8 Relationship between first natural frequency/stiffness and parameters (t and l)

Fig. 9 Finite element model

Fig.10 Modal analyses results

Fig.11 Experimental setup for stiffness test

Fig.12 Static stiffness of the positioning platform

Fig.13 Experimental setup for modal analysis

Fig.14 Frequency responses of the X and Y axes

Fig.15 Experimental setup of workspace test

Fig.16 Workspace of the platform

Fig.17 Hysteresis loop and coupling motion of the platform

Table 1 Material and physical parameters

Table 2 Optimization results of PSO and GA

Table 3 Ranges of the parameters and frequency

Table 4 Results and error of stiffness

Table 5 Comparisons of natural frequency in the X direction

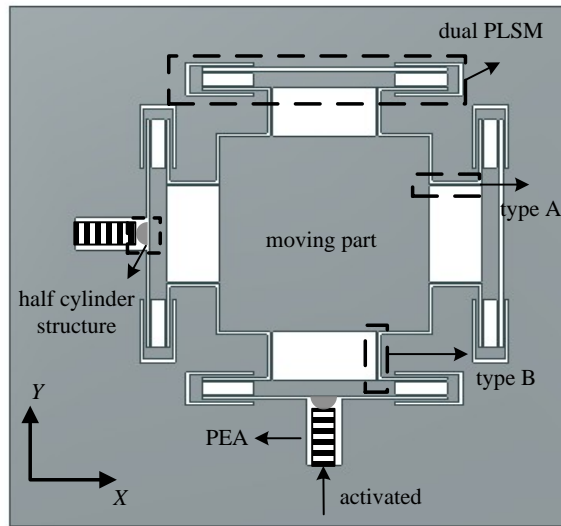


Fig.1 Schematic diagram of the 2-DOF precision positioning platform

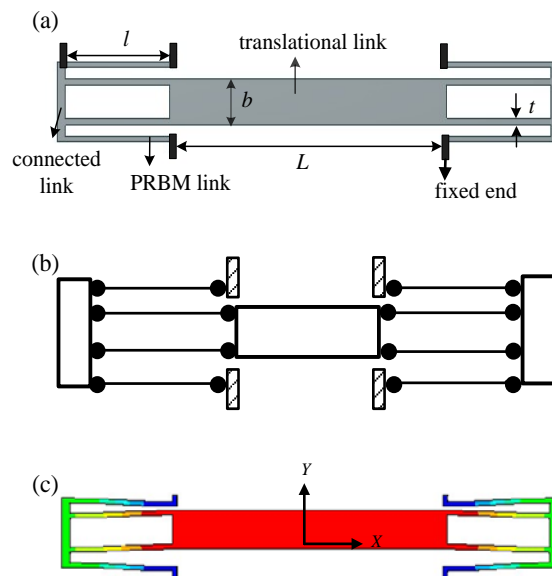


Fig.2 PLSM mechanic model a) Schematic diagram of dual PLSM b) Equivalent model of dual PLSM c) Displacement of dual PLSM

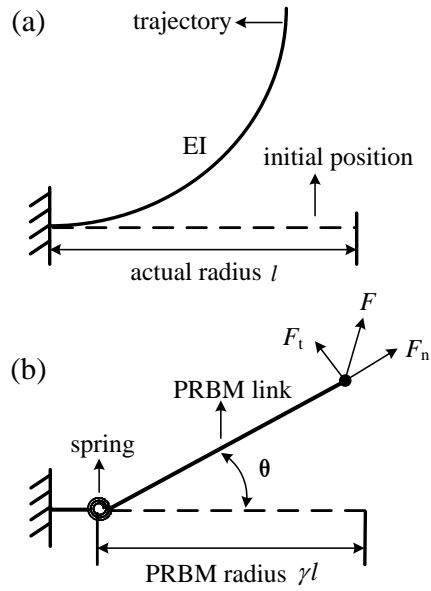


Fig.3 PRBM model of link a) The actual deformation of link b) The deformation of PRBM link

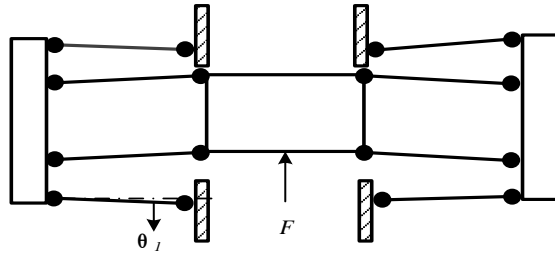


Fig.4 Rotational angle θ_I due to the force F

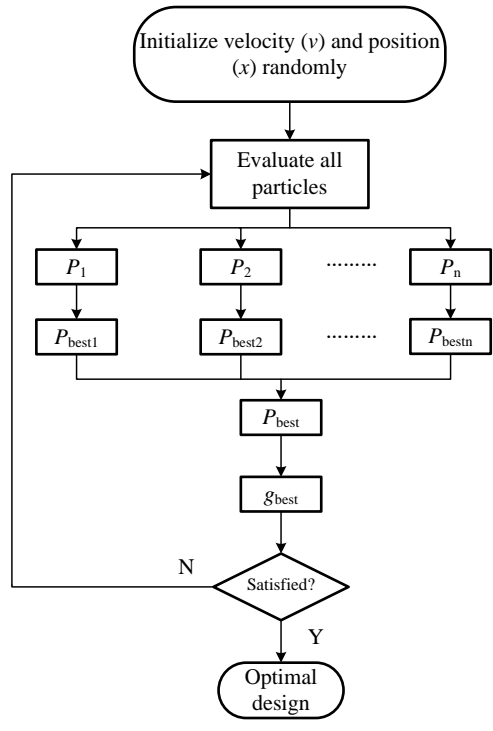


Fig.5 Flowchart of the PSO optimization approach

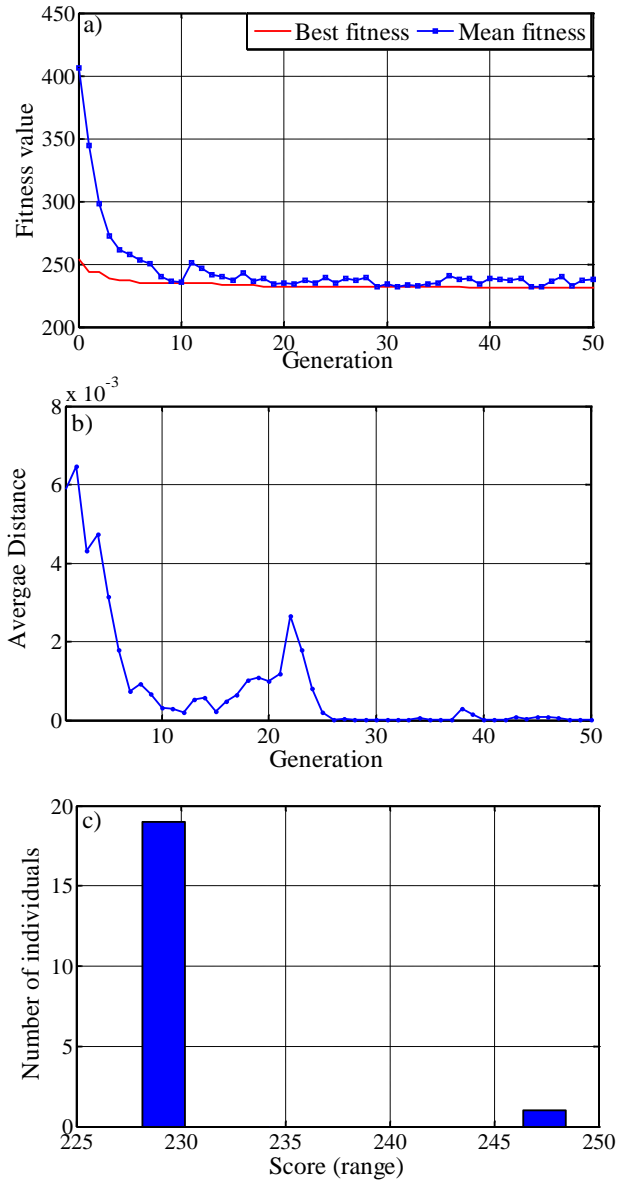


Fig.6 PSO optimization process a) Converge process of PSO b) Average distance between individuals c) Score histogram

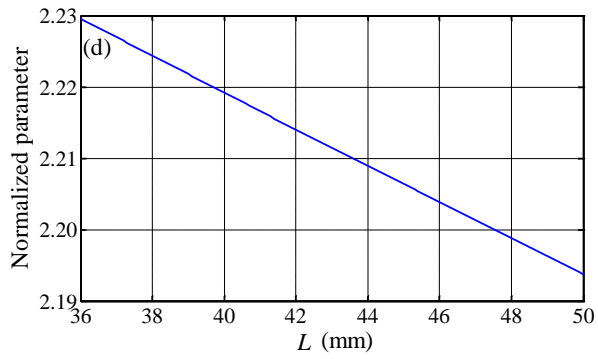
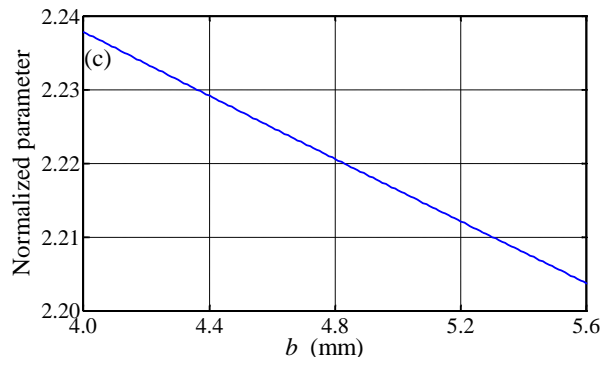
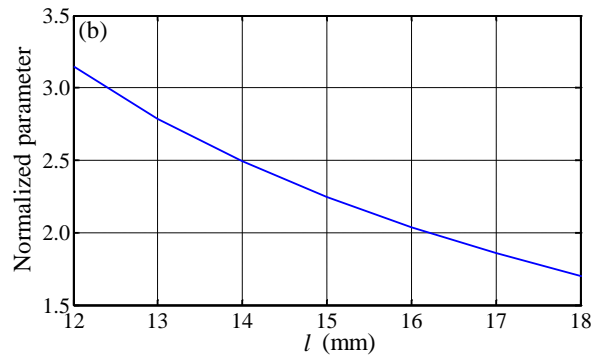
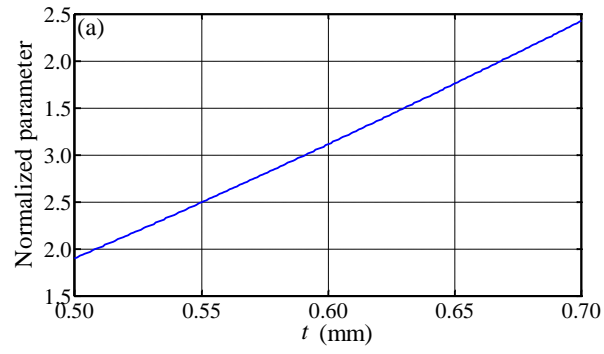


Fig.7 Relationship between the geometric parameters and the first natural frequency

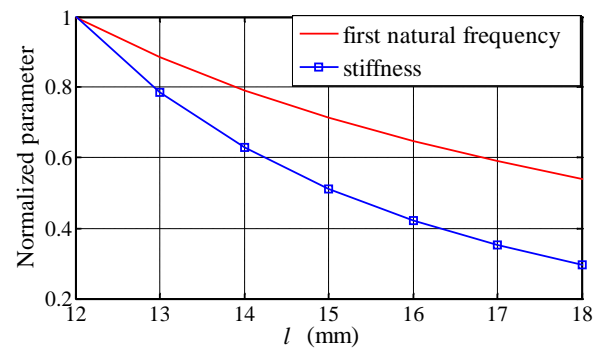
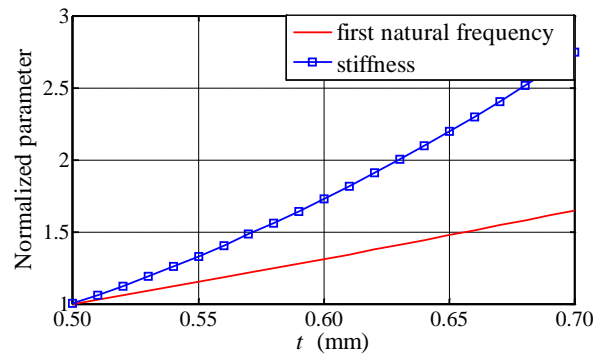


Fig.8 Relationship between first natural frequency /stiffness and parameters (t and l)

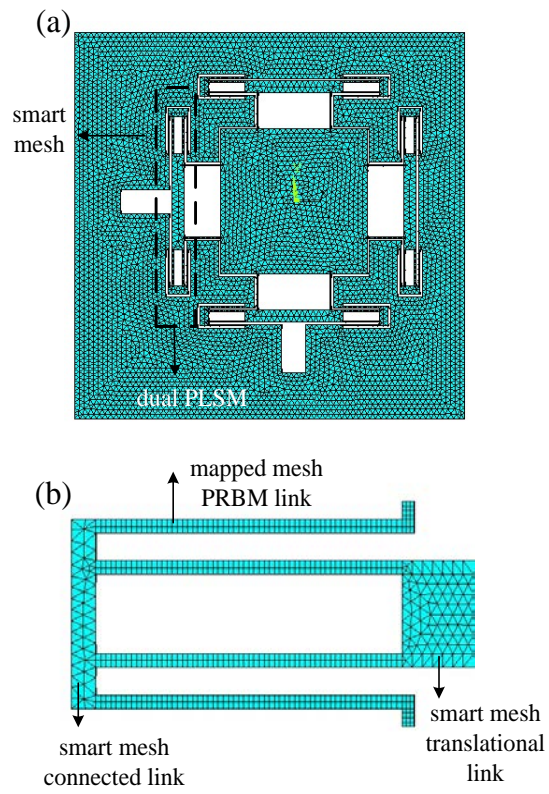


Fig. 9 Finite element model a) platform b) dual PLSM

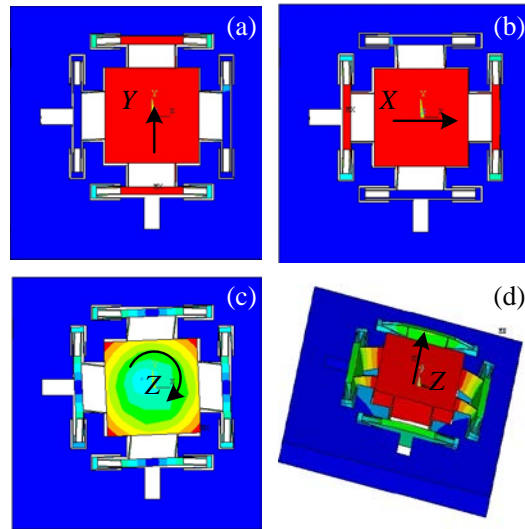


Fig.10. Modal analyses results (a)1st mode shape (235Hz) (b)2nd mode shape (235Hz) (c)3rd mode shape (713Hz) (d)4th mode shape (1568Hz)

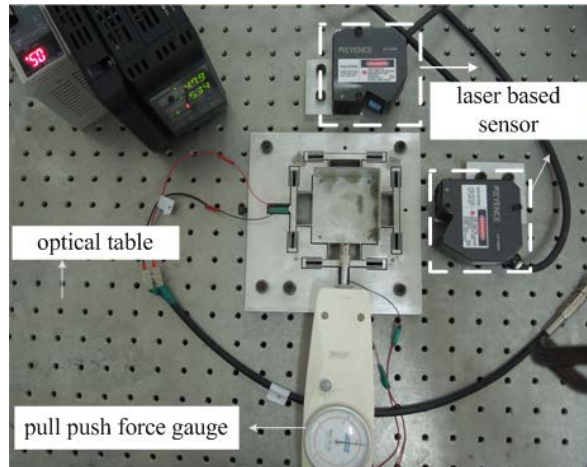


Fig.11 Experimental setup for stiffness test

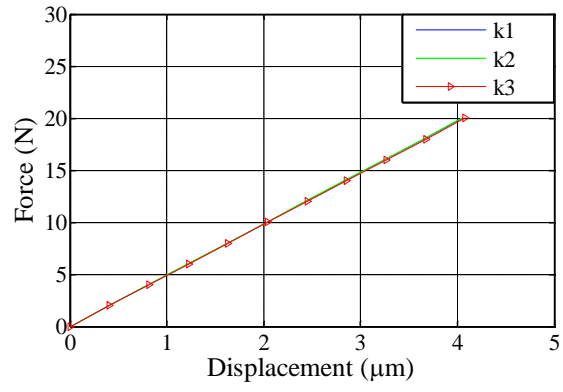


Fig.12 Static stiffness of the positioning platform

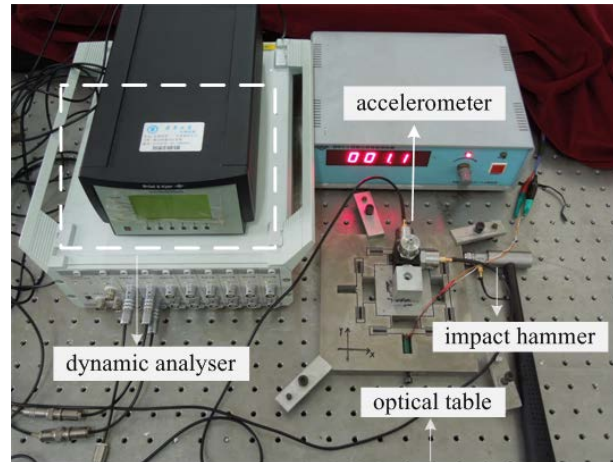


Fig.13 Experimental setup for modal analysis

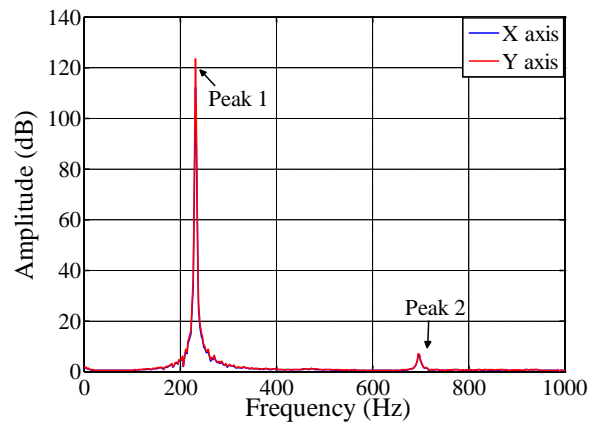


Fig.14 Frequency responses of the *X* and *Y* axes

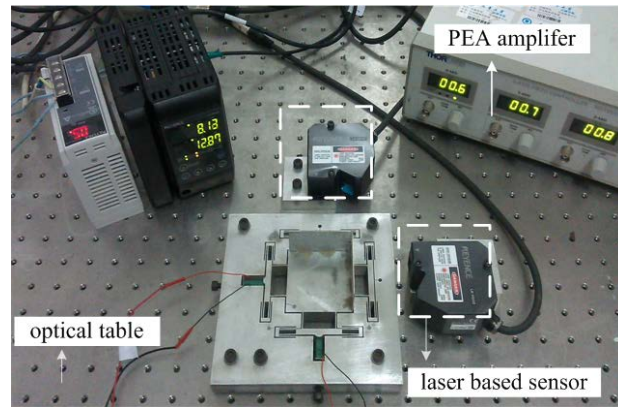


Fig.15 Experimental setup of workspace test

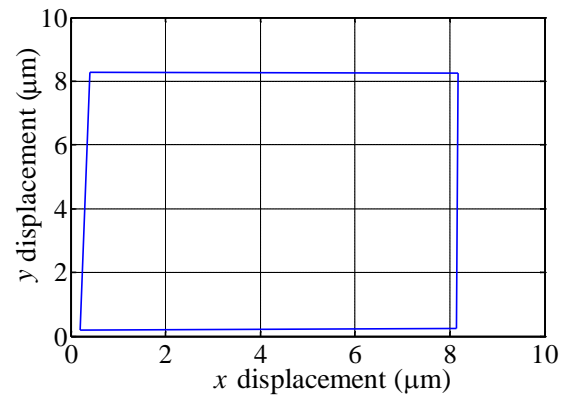


Fig.16 Workspace of the platform

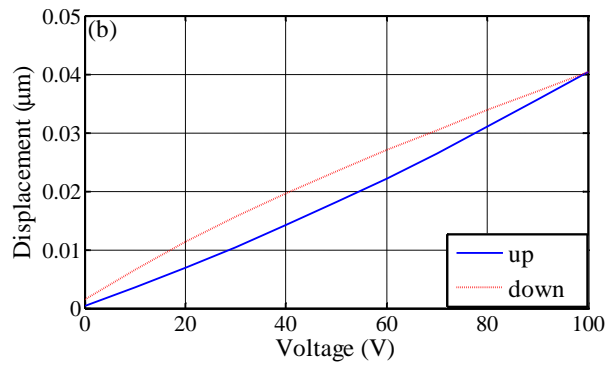
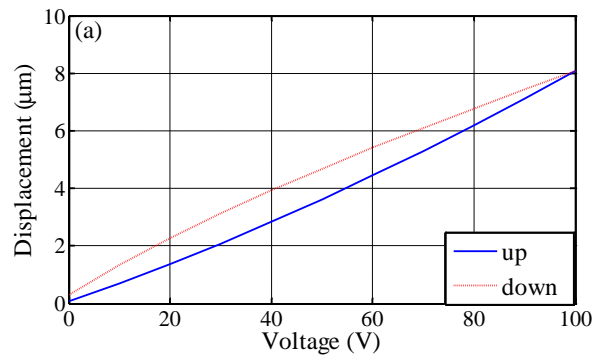


Fig.17 Hysteresis loop and coupling motion of the platform a) The motion in Y direction b) The motion in X direction

Table 1 Material and physical parameters

$E/(\text{N/m})$	0.7×10^{11}
$\rho/(\text{kg/m}^3)$	2700
$k_{\theta}/(\text{Nm/rad})$	2.68
γ	0.85
$m_3/(\text{kg})$	0.004
$m_4/(\text{kg})$	0.5
$d/(\text{mm})$	18

Table 2 Optimization results PSO and GA

Parameter	PSO	GA
$L/(\text{mm})$	40.0	42
$b/(\text{mm})$	5.0	5.2
$l/(\text{mm})$	15.0	16
$t/(\text{mm})$	0.63	0.57
$f/(\text{Hz})$	231.4	209.6

Table 3 Ranges of the parameters and frequency

	Lower bound	Upper bound	Freq.change
$t/(\text{mm})$	0.50	0.70	1.0
$l/(\text{mm})$	12.0	18.0	1.5
$b/(\text{mm})$	4.0	5.6	0.032
$L/(\text{mm})$	36.0	50.0	0.035

Table 4 Results and error of stiffness

	Analytic	FEA	TEST	ERROR(%)
Stiff.(N/ μm)	4.92	4.90	4.97	1.01/1.21

Table 5 Comparisons of natural frequency in the X direction

	Analytic	FEA	TEST	ERROR(%)
Freq.(Hz)	229	235	231	0.87/1.73